ACS APPLIED MATERIALS & INTERFACES

Research Article

www.acsami.org

Highly Sensitive Reduced Graphene Oxide Impedance Sensor Harnessing π-Stacking Interaction Mediated Direct Deposition of Protein Probes

Kwang Su Kim,[†] Yu Mi Um,[‡] Ji-ryang Jang,[‡] Woo-Seok Choe,*[,†,‡] and Pil J. Yoo*[,†,‡]

[†]SKKU Advanced Institute of Nanotechnology (SAINT) and [‡]School of Chemical Engineering, Sungkyunkwan University, Suwon 440-746, Republic of Korea

Supporting Information

ABSTRACT: Graphene-based electrochemical impedance sensors have recently received much attention due to their outstanding sensing capability and economic viability. In this study, we present a novel means of constructing an impedance sensing platform via harnessing intrinsic π-stacking interactions between probe protein molecules and reduced graphene oxide (RGO) substrate, obviating the need for introducing external chemical groups often required for covalent anchoring of the probes. To achieve this goal, protein molecules used as a probe were denatured to render their hydrophobic residues exposed in order to facilitate their direct π-stacking interactions with the surface of RGO nanosheets. The protein molecules in denatured form, which would otherwise have difficulty in undergoing π-stacking interactions with the RGO surface, were found to uniformly cover the RGO nanosheets at high density, conducive to providing a graphene-based impedance sensing platform capable of detecting a probe-specific analyte at high sensitivity. The proof-of-concept performance of thus-constructed RGO-based impedance sensors was demonstrated via selective detection of biological binding events of antigen−antibody reaction at a femtomolar range. Notably, since the π-stacking interaction can occur on the entire RGO surface, it can desirably exclude a backfill process indispensable for the conventional biosensors to suppress background noise signals. Since the procedure of π-stacking mediated direct deposition of on-purpose denatured protein probes onto the RGO surface is facile and straightforward, the proposed strategy is anticipated to extend its applicability for fabrication of high performance graphene-based bio or chemical sensors.

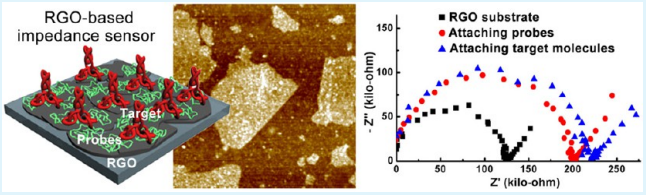

KEYWORDS: *electrochemical impedance spectroscopy, biosensors, reduced graphene oxide, π-stacking interactions, proteins, denaturation*

Graphene, a two-dimensional sheet structure of sp^2 conjugated atomic carbon, has attracted considerable attention in a myriad of research works due to its outstanding electronic, electrochemical, and thermal properties.[1,2] As a result, its novel characteristics have led to a broad range of device applications in transistors,[3] solar-cells,[4] supercapacitors,[5] and sensors.[6,7] In addition, an excellent biocompatibility[8] also facilitates its complexation with biomaterials such as DNAs,[9] aptamers,[10] peptides,[11] enzymes,[12,13] and proteins.[14] Among various applications, graphene-based biosensors have been extensively investigated to selectively detect various analytes at high sensitivity using fluorescent or electrochemical methods.[15−17] In terms of the electrochemical approach, in particular, electrochemical impedance spectroscopy (EIS) has been widely exploited where interfacial impedance changes upon biorecognition events occurring at the interface between the surface and electrolytes are sensitively measured.[18−20] After an attachment of probes on the electrode, an interfacial charge transfer resistance (R_{ct}) increases, which is expressed by electrical information in the frequency domain.[21] Therefore, a direct and strong immobilization of probes on a graphene surface is necessary for a fabrication of highly sensitive graphene-based impedance biosensors. However, since the graphene surface comprising only carbon atoms is quite hydrophobic and electrostatically neutral, chemical or physical binding of probes directly atop the unmodified graphene surface is rarely attainable.

Meanwhile, for the case of small biomolecules frequently employed as probes to specifically capture target analytes, noncovalent bindings including π-stacking interaction are likely to occur, in principle, directly on the graphene surface due to the availability of nonpolar or aromatic ring containing groups enriched in these biomolecules.[22,23] However, π-stacking mediated direct assembly of these probe biomolecules has rarely been reported since these biomolecules have been evolved in nature to be shaped into higher order structures conducive to be hydrated in an aqueous environment. Moreover, direct interfacing of relatively large biomolecules such as proteins with the graphene surface is more challenging

Received: December 25, 2012
Accepted: April 3, 2013
Published: April 3, 2013

   dx.doi.org/10.1021/am303238r | ACS Appl. Mater. Interfaces 2013, 5, 3591−3598

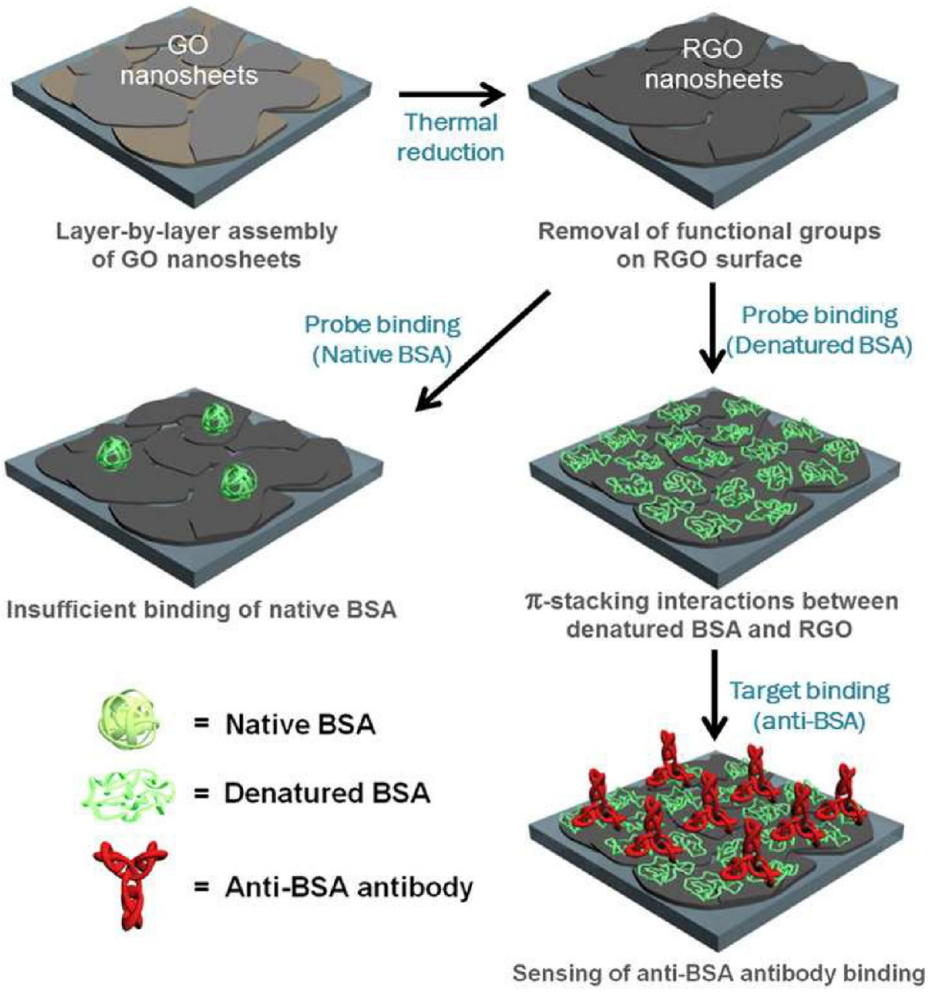

Figure 1. Schematic of constructing the sensing platform based on π-stacking interactions between probes and the RGO surface.

since a majority of proteins found in vivo in their native forms also exhibit exquisite three-dimensional structures where strategic positioning of individual amino acid residues is optimized to suit their biological activity and/or thermodynamic stability in water-rich milieu. Hence, this exteriorly revealed hydrophilic nature hampers their direct π-stacking interactions with the hydrophobic graphene surface. As an attempt to overcome this limitation, the use of graphite oxides (GOs) as an interlinking layer has been widely pursued,[24] wherein hydroxyl, carboxylic, or epoxy functional groups are introduced to further accommodate various biomolecular probes via covalent bonding or electrostatic interactions. However, due to the intrinsically nonelectroconductive characteristic of GOs, the introduction of a GO layer on a top surface often necessitates separate pretreatment of an underlying electroconductive substrate, which usually makes the system more complicated.

To address this point, counterintuitively, our strategy aims at utilizing a denaturation of proteins to generate the π-stacking interactions, instead of adopting functional groups to the GO surface. Despite the presence of localized electrostatic charge on the native protein surface, protein molecules are prone to form aggregates, mostly via inter- or intramolecular π-stacking interactions mediated by their surface exposed hydrophobic patches once they are subjected to denaturing conditions. Furthermore, in the presence of a hydrophobic stationary phase, native proteins of high surface hydrophobicity and denatured proteins tend to adsorb strongly on the hydrophobic surface to minimize the interfacial area in contact with water, which is the underpinning principle for hydrophobic interaction chromatography. Hence, it is tempting to investigate the possibility if this phenomenon would possibly enable the denatured proteins to make direct interactions with the aromatic groups on the graphene surface.

In this work, we utilize thermally reduced graphene oxide (RGO) thin films as a working electrode in electrochemical impedance sensors for inducing π-stacking interactions between denatured protein probes and the RGO surface. The RGO films are prepared by alternately applied deposition of oppositely charged GO nanosheets using spin-assisted layer-by-layer (LbL) assembly method, followed by a thermal reduction process. As a model probe, bovine serum albumin (BSA) is used following denaturation via chemical or thermal treatment to enable its direct adsorption onto the RGO surface by π-stacking interactions. A successful attachment of BSA probes is confirmed by monitoring the topological change on the surface by atomic force microscopy (AFM), Raman spectra, and EIS data. Further binding on the immobilized BSA probes through an antigen−antibody reaction with anti-BSA antibody is also confirmed by EIS measurement, resulting in high sensitivity in the tens of femtomole regime at the minimum. Notably, nonspecific binding of other hydrophilic biomolecules

is effectively screened on the surface of the BSA-covered RGO electrode, which is proven by comparative studies of applying the identical concentration of anti-BSA antibody in crude cell lysate solution or the mouse serum. Therefore, this approach enables the implementation of a novel sensing platform with a high sensitivity and selectivity while excluding the need for backfill processes to prevent the sensor surface from nonspecific binding and contamination. Overall, it is anticipated that the obtained advantages as a robust operability in sensing platform and high precision in sensitivity are widely accepted for the conventional biosensors and biodevices.

EXPERIMENTAL SECTION

Materials. A detailed description of the materials information and synthetic procedure for preparing the positively and negatively charged GOs is outlined in our previous study.[25] Bovine Serum Albumin (BSA, A7906, Sigma-Aldrich) was dissolved in tris-(hydroxymethyl)-aminomethane (Tris, A2264, AppliChem, Germany) buffer solution. Urea (U0021, Samchun Chemical, Korea) and DL-dithiothreitol (DTT, M109-5G, amresco, USA) were used as denaturants (i.e., ureas as a chaotrope and DTT as a reducing agent, respectively) during chemical denaturation treatment. For high-performance liquid chromatography (HPLC) analysis to confirm protein denaturation, HPLC grade solvents of acetonitrile (A1764, Samchun Chemical, Korea), trifluoroacetic acid (TFA, 302031, Sigma-Aldrich, USA), and tryptone (1612, Conda, Japan) were used as received.

Preparation of Thermally Reduced GO Substrate. Quartz substrates were first cleaned with sonication in acetone, ethanol, and deionized (DI) water and then were plasma-treated (<30 W, 0.1−0.5 Torr, PDC-001, Harrick Scientific Corp., NY) for 2 min to produce a negatively charged surface. The spin-assisted LbL-assembly of charged GO nanosheets was conducted using a spin-coater (Midas system, Spin-1200D, Korea). The solutions of oppositely charged GOs were alternatively spun coated (30 s at 2000 rpm) onto the quartz substrates with two additional washing steps with deionized water between the layer deposition steps. Finally, the assembled graphene oxide film was thermally reduced in a furnace in an inert environment with H_2/Ar (1:3) purging at 720 °C.

Protein Denaturation and Surface Binding. An overall procedure for the protein probe binding on RGO assembled surface is schematically presented in Figure 1. Chemically denatured BSA was prepared by incubating native BSA of varying concentrations in denaturation buffer (20 mM Tris, 6 M urea, 5 mM DTT, pH 7.5) for 5 h at 25 °C. As a control, native BSA was prepared in Tris buffer lacking denaturants (20 mM Tris, pH 7.5). For immobilizing BSA probes on the RGO substrate, 1 mL of solution containing native or chemically denatured BSA molecules was drop-dispensed on the RGO film and the film was incubated for 6 h at 25 °C. For direct deposition of thermally denatured BSA on the RGO surface, thermal denaturation of BSA and surface immobilization were concurrently conducted by incubating 1 mL of native BSA solution on the RGO film for 10 min at 95 °C in order to avoid self-aggregation of the denatured BSA molecules.

Following adsorption of native or denatured BSA probes on the RGO, unbound BSA molecules, and residual buffer species were removed by washing with DI water. Anti-BSA antibody (B2901, Sigma-Aldirich) was diluted to the predetermined concentrations (0.025−100 pM) with 20 mM Tris buffer. The performance of a graphene impedance sensor was assessed by recording the interfacial charge transfer resistance change (ΔR_{ct}) arising from probe−analyte (antigen−antibody) reaction. For this, the RGO films conjugated with thermally denatured BSA were incubated in anti-BSA antibody solution for 30 min at 4 °C prior to ΔR_{ct} measurement. In order to evaluate specificity of the graphene-based impedance sensor in view of selective recognition of the target analyte, impedance measurement was also conducted against cocktail solutions containing a known amount of anti-BSA antibody in the presence of diverse potential interferents extracted from bacterial cells (e.g., nucleic acids, host cell proteins, and endotoxin). To prepare the cocktail solutions, *E. coli* BL21 (DE3) cells were grown on 200 mL Luria−Bertani (LB) medium (10 g/L tryptone, 10 g/L yeast extract, 5 g/L NaCl) in a shaking incubator at 250 rpm, 37 °C for 16 h. Grown cells were mechanically disrupted using a one shot disrupter (Constant Cell Disruption System, UK) at 21 kpsi and 4 °C. Following cell disruption, the cell lysates were centrifuged at 15 000*g* and 4 °C for 25 min to remove cell debris. Then, the supernatant fraction with a total protein concentration of 0.5 g/L via Bradford assay was mixed with known amounts of the analyte to give the cocktail solutions. Mouse serum used in this study was used as received (Woojung Biomedical Science Community, Inc., Korea). Total amount of proteins measured by Bradford assay in mouse serum is 50 g/L and it was used after 100 times dilution with Tris buffer solution.

Measurements and Characterizations. The surface topology of the RGO films was investigated using atomic force microscopy (AFM, Dimension 3100, Veeco, Plainview, NY) in tapping mode under dry conditions. To visualize the difference after immobilization of denatured BSA, a thin layer with 0.5 bilayer of thermally reduced GO film on a wafer substrate was used for AFM observation. Impedance measurements were carried out in 0.1 M KCl without a redox couple. A conventional three-electrode system comprising a platinum wire as a counter electrode, an Ag/AgCl as a reference electrode, and the graphene film as a working electrode was employed. A frequency was varied from 0.1 to 10^6 Hz. The amplitude of the applied sine wave potential in each case was 10 mV. The extent of BSA denaturation was analyzed by HPLC (1525 Binary HPLC Pump, 2998 PDA Photodiode Array, Waters, MA) equipped with a C5 reverse phase column (5 μm, 300 Å, 150 mm × 4.6 mm, Jupiter, Phenomenex, CA). Each protein sample before and after the denaturation treatment was filtered using 0.2 μm cellulose acetate filter (25CS020AS, Advantec, Japan). Following 20 μL injection, a step gradient (5−95%) using acetonitrile−water with 0.1% (v/v) trifluoroacetic acid was applied at a flow rate of 1 mL/min for 20 min for elution of the proteins. Raman spectra were taken using a Raman spectrometer system (SENTERRA Raman Microscope, Bruker, MA) to confirm the π-stacking interactions between denatured BSA and RGO surface.

RESULTS AND DISCUSSION

In order to prepare the graphene electrode surface, one should generally come up with monolayered graphene films prepared by chemical vapor deposition (CVD) method based on Cu-foil catalyzed synthesis and subsequent transfer on a target substrate, which can exhibit outstanding charge transport capability adequate for applications in transparent electrode or electronic devices. In terms of an electrochemical sensing system, however, excessively high charge transport characteristics of the electrodes can be partly disadvantageous in detecting a subtle electrochemical change at the electrode surfaces. For example, in graphene-based impedance biosensors, the surface-immobilized biomolecule on graphene electrode interrupts the current passage transported from the counter electrode, causing a decrease in the amount of electrical charge that can be delivered to the underlying graphene surface. In the case of using CVD-grown graphene layers for impedance sensors, the electrical charges transported on the electrode surface can rapidly pass through undergoing little resistance owing to the flawlessly constructed interconnections of carbon atoms at the electrode surface, which is insufficient to generate a discernible change in R_{ct} value in EIS data (details will be discussed in the later part).

This contradictory characteristic of graphene electrode prepared by CVD method can be resolved by adopting the layered interconnected structure of graphenes based on RGO self-assembly. In contrast to the monolayered structure of CVD-grown graphene films, the RGO-based films consist of a

stacked structure of graphene nanosheets, requiring a multilayer-assembled structure for complete surface coverage with forming random networks. Although the electrical conductivity is inferior to that of CVD-grown graphene films, since the intersheet hopping mechanism of the electrical charge is allowed within the stacked layers, it rather imparts a greater sensitivity in R_{ct} value when used as an electrochemical impedance sensing system. To fabricate the RGO-assembled graphene layers, we first synthesized the oppositely charged GOs; one is carboxylic acid-functionalized GOs (GO−) and the other is amine-functionalized GOs (GO+, converted from GO− by sequential acyl chlorination and amidation reactions) prepared according to the previously reported procedures.[25] Then, the electrostatic assembly between positively charged and negatively charged GOs was conducted alternately. In particular, instead of conventionally used dipping-based LbL assembly, a spin-assisted LbL assembly method is used here to minimize the surface roughness by suppressing the nucleation and self-aggregation of GO nanosheets on the substrate. To verify this characteristic, the surface topology of the GO-assembled films was observed with AFM as shown in Figure 2.

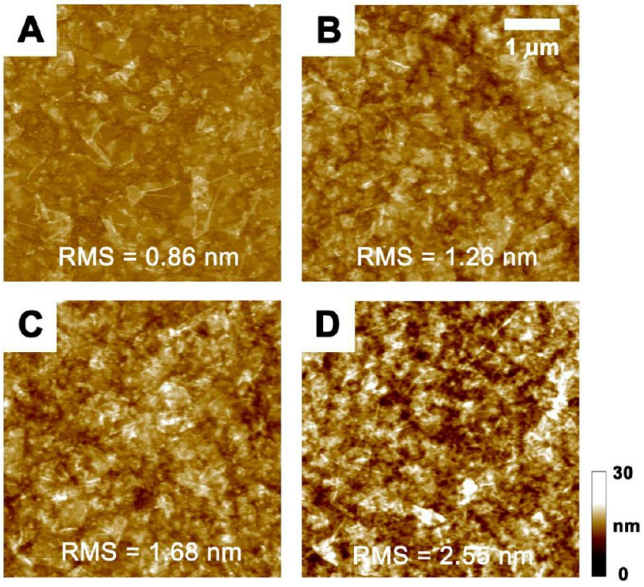

Figure 2. Two-dimensional AFM images of LbL-deposited GO films (scan size = 5 μm × 5 μm) with varying bilayer numbers. (A) One bilayer. (B) Two bilayers. (C) Three bilayers. (D) Four bilayers. Root-mean-square (RMS) roughness of the surface increases with increasing deposition numbers.

When a single bilayer is deposited (Figure 2A), both structures of pristine platelets of GO− and broken-up sheets with tattered edges of GO+ are observed, indicative of successful occurrence of GO binding through electrostatic interactions. However, since a complete surface coverage has not yet been achieved, it cannot be directly used as an impedance sensing platform under the given condition. When an additional bilayer is deposited (Figure 2B), on the other hand, the entire surface is now completely covered with GO nanosheets. Upon further increasing the bilayer numbers (Figures 2C and 2D), however, the GO-assembled surfaces exhibit a greater surface roughness, making it impractical for a selective binding with probes or analytes due to increased possibility of nonspecific adsorption on rough surfaces. Then, the GO-assembled films are thermally annealed at 720 °C in Ar environment with a small addition of hydrogen to remove the surface functional groups from GO nanosheets, which finally leads to a conversion to the RGO films. We also confirm that there is no noticeable roughness variation after thermal annealing and reduction process, implying that a possibility of the film densification and topological change due to the loss of functionalities of GO nanosheets can be negated.[25]

One notable advantage of LbL-assembled RGO films is that their electrochemical properties can be elaborately manipulated by varying the deposition numbers. To get a tunability over the interfacial resistance, EIS data were obtained with varying the bilayer deposition numbers (Figure 3). It is expected that R_{ct}

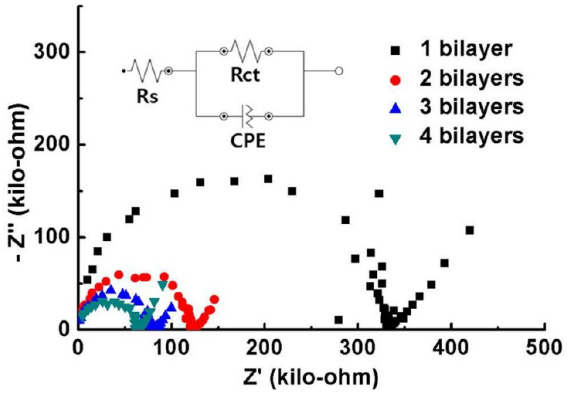

Figure 3. Normalized Nyquist plot of RGO films with varying bilayer deposition numbers from 1 to 4. (inset) Equivalent circuit used in a conventional three-electrode system without redox probes (R_{ct} charge transfer resistance, CPE constant phase element, R_s electrolyte solution resistance).

values will be reduced in response to an increase in the deposition number due to the facilitated charge passage through randomly formed networks within the stacked RGO nanosheets. In the EIS data, the semicircle portion observed at high frequency range corresponds to the charge transfer limiting process. Therefore, the interfacial charge transfer resistance, R_{ct}, can be directly measured as the semicircle diameter. As shown in Figure 3, a single bilayer-deposited film exhibits a deformed semicircle and accordingly results in irregularly defined R_{ct} because of an incomplete surface coverage of graphene nanosheets as presented in Figure 2A. However, additional bilayer deposition enables the graphene films to have a consistent R_{ct} value for repeatedly prepared samples, implying a uniform surface coverage with RGO nanosheets. Further deposition conditions to 3−4 bilayers lead to more stabilized and smaller values in R_{ct}, whereas the increased surface roughness due to the random accumulation and folding of RGO nanosheets can disadvantageously give rise to the increased nonspecific adsorption of analyte species. Therefore, in this study, the optimized number of bilayer depositions is fixed at two; under such a condition, a uniform value in R_{ct} while maintaining a minimized surface roughness can be simultaneously achieved.

As mentioned in the introduction part, GO-assembled films have been extensively exploited for sensing applications since GO has a number of negatively charged functional groups on the edges as well as on the basal plane in a broad pH range.[26] This property readily facilitates the attractive binding with proteins containing positively charged amine functions. The

RGO, by contrast, loses its charged functions during the thermal reduction process, which eventually renders non-reactive neutral surfaces with hydrophobic characteristic. Since the exterior of native proteins is highly hydrophilic, the RGO surface rarely allows interactions with probes of native proteins. Therefore, an alternative approach harnessing denatured proteins, whereby the inner hydrophobic aromatic residues can be outwardly exposed, is desirable to generate stable yet scalable π-stacking interactions of probes with the RGO surface. In order to obtain a validity of this approach, here, we utilize bovine serum albumin (BSA) as a model probe which is a nonspecific globular protein while holding merits of bio-chemical stability and supplying abundance.[27]

Among various protein denaturation methods, the two most widely used treatments (i.e., chemical and thermal) were employed to denature BSA probe molecules. First, for chemical denaturation, DTT and urea are used as denaturants. The former cuts disulfide bonds without significantly disturbing the three-dimensional structure of BSA, leading to a localized change in the chain conformation. The latter prevents the denatured BSA (dBSA) from aggregation in the buffer solution as well as restoration to the native form. Meanwhile, due to a relatively high concentration of urea, π-stacking interactions of dBSA molecules through the exposed hydrophobic patches with the RGO surface can be substantially interrupted. Therefore, dBSA prepared by chemical treatment requires prolonged incubation time (e.g., 6 h) prior to reaching equilibrium binding on the RGO surface. On the other hand, thermal denaturation of protein molecules is generally irreversible and occurs more explosively to reach its equilibrium status of insoluble aggregates. Therefore, both BSA probes and RGO substrate were simultaneously immersed in solution at an elevated temperature of 95 °C for a short period of time (e.g., 10 min). This is to direct dBSA probes to participate more actively in π-stacking interactions with the RGO surface while suppressing the self-aggregation of dBSA molecules into insoluble aggregates.

In order to confirm the denaturation of BSA molecules for each denaturation route, RP-HPLC analysis was conducted. As shown in Figure 4, native BSA is eluted at 11.8 min and dBSA subjected to chemical denaturation is eluted at 12.7 min, indicative of the presence of surface exposed hydrophobic amino acid residues likely to interact more strongly with the stationary reverse phase. For dBSA following the thermal treatment, neither a native nor denatured peak was observed due to the complete irreversible conversion of native BSA to insoluble dBSA aggregates which was filter-eliminated from the sample prior to RP-HPLC injection. On the basis of these results, we confirm that a majority of BSA molecules are successfully denatured both in chemical and thermal methods.

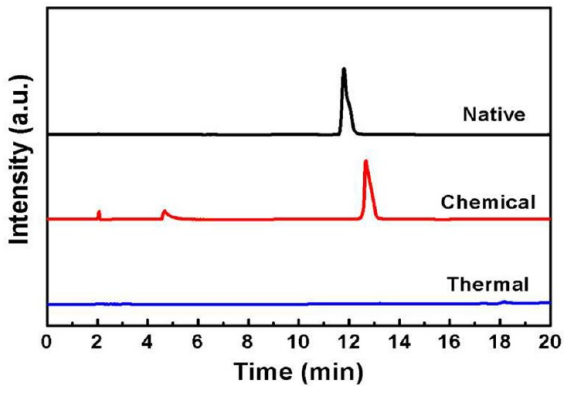

Figure 4. RP-HPLC peak responses for native and denatured (chemically or thermally) forms of BSA.

To verify the facilitated dBSA binding on the RGO surface by π-stacking interactions, the EIS analysis was performed for the RGO electrodes incubated with dBSA at varying concentrations. As revealed in Figure 5, since the R_{ct} increment

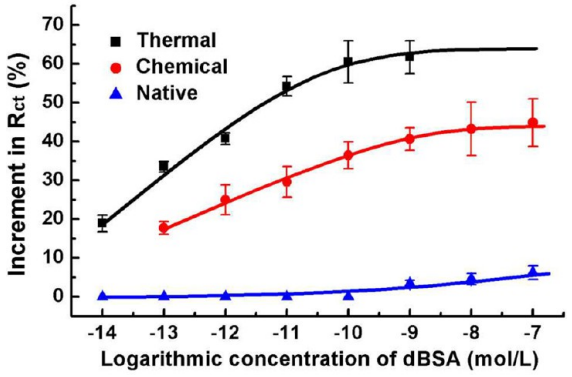

Figure 5. Plot of percent increment in R_{ct} vs logarithmic concentrations of denatured BSA.

strongly depends on the surface coverage of BSA on RGO surface, highly enhanced surface binding characteristic and subsequent large increases in R_{ct} are observed for the dBSA deposition in a concentration dependent manner. In contrast, the native form of BSA makes no noticeable change in the R_{ct} value (less than 5% in R_{ct} increment is observed even with an incubation time of 6 h), indicative of efficiently expelling the hydrophilic moieties from the RGO surface. Along with this notable selectivity for π-stacking interactions, a change in R_{ct} values is more pronounced for dBSA subjected to heat treatment, implying the enhanced π-stacking interactions in the absence of intervening chaotropic denaturant molecules such as urea. When denaturant species is applied, however, the facilitated surface binding of dBSA is apparently disturbed and retarded. The saturation points of dBSA binding on the RGO surface which correspond to the plateau in R_{ct} values are observed to be ~100 pM for thermal dBSA and ~10 nM for chemical dBSA, respectively, manifesting a more uniform and dense coverage of dBSA probes on the RGO surface for the case of thermal treatment.

Furthermore, surface topologies of the dBSA probe-treated samples were characterized by AFM analysis. As shown in Figure 6A, a pristine RGO nanosheet has a unit thickness of ~1 nm. When chemically denatured BSA is applied on the surface, the locally aggregated and irregularly bound globules with additional thickness of 1−2.5 nm are observed on the RGO nanosheets due to the urea-interfered π-stacking interactions (Figure 6B). On the other hand, when heat-denatured dBSA is used (Figure 6C), dBSAs are uniformly distributed over RGO nanosheets (additional thickness increase less than 0.5 nm) with high density. This proves the effectiveness of thermal denaturation route and the resulting facilitated π-stacking interactions between exposed hydrophobic residues of protein and the RGO surface. This result explains well the EIS data as to the greater increment in R_{ct} values for probe protein deposition on the RGO with thermal denaturation than those

dx.doi.org/10.1021/am303238r | ACS Appl. Mater. Interfaces 2013, 5, 3591−3598

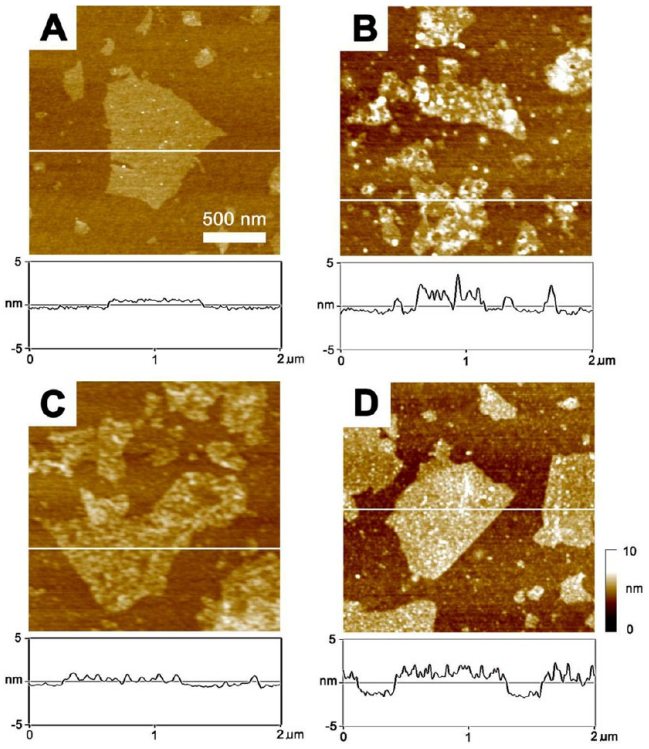

Figure 6. Two-dimensional and cross-sectional AFM observation of sequential binding of biomolecules on RGO surface (scan size = 2 μm × 2 μm). White lines indicate the sectioned regions. (A) Bare RGO surface. (B) Immobilizing chemically denatured BSA. (C) Immobilizing thermally denatured BSA. (D) Additional binding of anti-BSA antibody on thermal dBSA-treated RGO surface.

with chemically denatured BSA. Since the immobilized dBSA probes on RGO surface can play a role of capturing a biological recognition event, subsequently, anti-BSA antibody is applied on the dBSA-treated surfaces. Figure 6D shows that the layer of anti-BSA antibody with additional thickness of ~1.5 nm is uniformly formed on the thermal dBSA-covered RGO nanosheets. It should be noted that a small amount of anti-BSA antibody binding by nonspecific adsorption is observed in the background since the silicon substrate has not yet been fully passivated with RGO nanosheets typically for AFM characterization. To further ensure the dBSA binding on the graphene surface by π-stacking interactions, we deposited the thermal dBSA on the CVD-grown graphene (thickness less than 1 nm) and also observed the surface with AFM, confirming uniform dBSA deposition accompanied by a slight increase in the RMS surface roughness from 0.17 nm for a bare CVD-grown graphene to 0.48 nm after dBSA binding (see the Supporting Information).

Next, we performed the Raman spectra analysis for investigating the π-stacking interactions between dBSA and RGO surface. As shown in Figure 7, the dBSA-deposited wafer surface shows broad bands at 1309, 1448, 1595, and 1656 cm^{-1}, indicative of no specific occurrence of π-stacking interactions. In contrast, Raman spectra of carbon based materials displays two prominent peaks at ~1300 and ~1600 cm^{-1} (positions can vary depending on synthetic means and conditions), corresponding to the well documented D and G bands.[28] A monolayered CVD-grown graphene presents D and G band at 1351 and 1598 cm^{-1}, respectively. And a single-bilayered RGO surface also exhibits D and G bands at 1279 and 1602 cm^{-1},

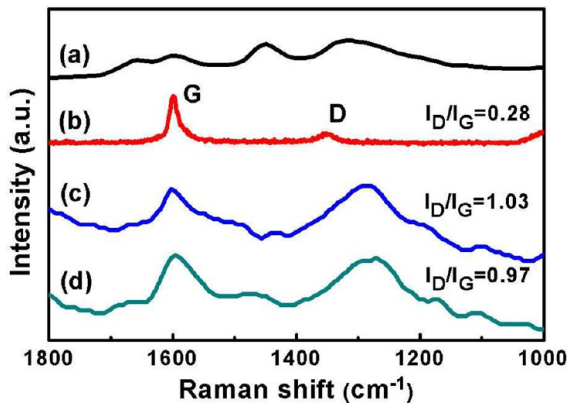

Figure 7. Raman spectra of dBSA (a), monolayered CVD-grown graphene (b), single-bilayered RGO (c), and thermal dBSA-immobilized RGO film (d) prepared on SiO_2 surfaces.

respectively. The structural and electrical properties of CVD-grown graphene and RGO can be quantitatively compared with the intensity ratio between the D and G bands (I_D/I_G). While the value of I_D/I_G for CVD-grown graphene is 0.28, the value substantially increases to 1.03 for the RGO surface. This difference in I_D/I_G suggests that the monolayered CVD-grown graphene has a well-ordered sp^2 network better than the RGO surface comprising multilayer stacked nanosheets, resulting in a lower electrical resistance.[29] After a binding of thermal dBSA onto the RGO surface, the Raman spectrum displays similar characteristics to that of RGO. However, because the contribution of dBSA comes into play, the Raman spectrum of thermal dBSA-covered RGO shows broader D and G bands compared to that observed in the pristine RGO. In addition, both D and G bands are blue-shifted slightly (1271 and 1595 cm^{-1}, respectively), which enables to confirm the facilitated π-stacking interactions between thermal dBSA and RGO surface.[30]

Now that the feasibility of harnessing the π-stacking interactions using RGO nanosheet-assembled surface is ensured, it remains for a comparative study with CVD-grown graphene surface to identify which one holds the superiority as an impedance sensing platform. Thermally denatured BSA of 100 pM concentration was applied on both CVD-grown graphene and RGO surface, by which surfaces can be mostly covered with dBSA probes through π-stacking interactions. As shown in Figure 8, the increased ratio in R_{ct} values is measured as 30% for CVD-grown graphenes, whereas 62% for RGO nanosheets-covered ones. Moreover, the semicircle in EIS is not fully developed for the CVD-grown graphene layer due to the low surface resistivity. By contrast, upon employing the RGO nanosheets into stacked structures, electrons supplied from the electrolytes are transported by interfacial hopping mechanism (tunneling current) between individually stacked RGO nanosheets, thereby enhancing the sensitivity in impedance variance. Moreover, the multilayer-stacked structure of RGO provides extra sites of edges/steps for binding with target species. This result is consistent with the "intersheet-effect" reported in the literature.[31]

As has been already demonstrated in Figure 6D, dBSA-covered RGO surface can be exploited as a sensing platform for detecting further biological binding, which is expressed as an additional increase in R_{ct} value of EIS data. In particular, BSA molecules include a specific amino acid sequence for binding with anti-BSA antibody. Since this epitope does not have

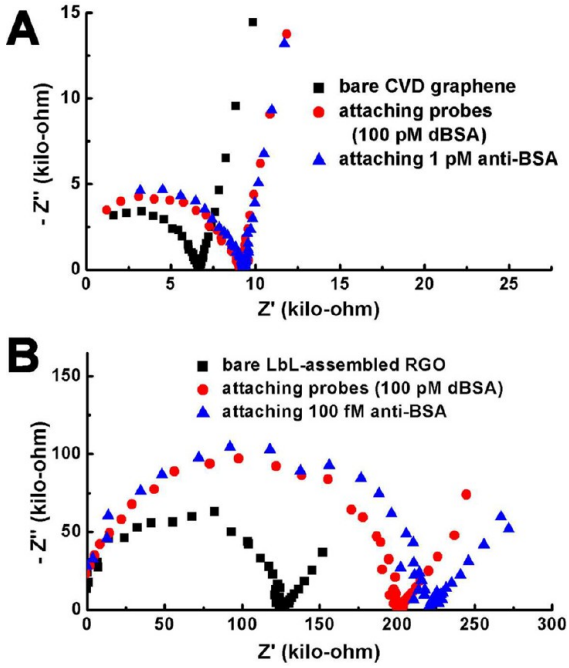

Figure 8. Comparison between CVD-grown graphene and LbL-assembled RGO films in EIS data responses after a surface binding of thermally denatured BSA and subsequently applied anti-BSA anibody.

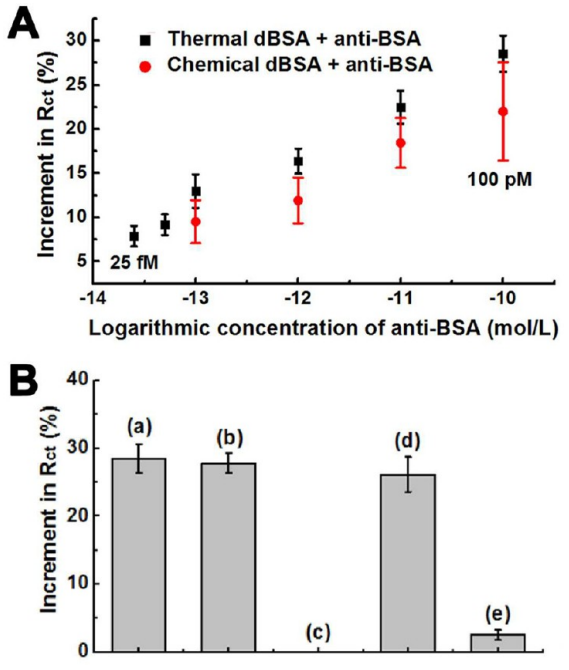

Figure 9. (A) Plot of increment in R_{ct} vs logarithmic concentrations of anti-BSA antibody. (B) Comparison of mean values in R_{ct} increment upon applying the (a) anti-BSA antibody, (b) anti-BSA antibody in cell lysate solution, (c) crude cell lysate solution only, (d) anti-BSA antibody in mouse serum solution, and (e) mouse serum solution only. Concentrations of anti-BSA antibody, cell lysate, and mouse serum are 6.6 μg/L, 0.5 g/L, and 0.5 g/L, respectively.

relevance to the three-dimensional structures of BSA, irrespective of the form whether being native or denatured, BSA molecules retain their affinity to the anti-BSA antibody.[32] However, due to the observed advantage of uniform and dense surface coverage (Figure 6C), the RGO surfaces treated with thermal dBSA probes are used as the electrode for detecting anti-BSA antibody. The dBSA-covered surface was incubated in Tris buffer containing varying concentrations of anti-BSA antibody for 30 min prior to assessing ΔR_{ct}. Since the molecular weight of the antibody (M_W = 160 000) is 2.5 times larger than that of BSA (M_W = 66 000), a substantial change in R_{ct} value can be measured, which is indicative of an increased hindrance in charge transfer from electrolyte to electrode. As shown in Figure 9A, the detection limit of anti-BSA antibody was measured as 25 fM with an R_{ct} increase of 7.9%. Control experiments were also carried out by incubating anti-BSA antibody onto bare RGO surfaces, exhibiting no noticeable antibody binding. This can be attributed to the lack of nonspecific background binding between antibodies with hydrophilic nature and inert hydrophobic RGO surface, similar to the case observed for native BSA. Therefore, the obtained performance in selectivity confirms that π-stacking interaction mediated probe molecule deposition on RGO nanosheets can be exploited to construct a useful graphene-based sensing platform.

Along with the sensitivity issue, high selectivity is necessary for sensing devices. In order to demonstrate the specificity of anti-BSA antibody binding, 100 pM (6.6 μg/L) antibody in bacterial cell lysate or mouse serum solution was applied on the dBSA-treated RGO surfaces. As shown in Figure 9B, resulting EIS data reveals that there is little difference in the increment of R_{ct} values irrespective of the type of antibody solutions. This outstanding selectivity can be attributed to a complete surface coverage of dBSA probes on the RGO surface that effectively excludes a concern of nonspecific binding of various interfering species crowded in the cell lysate or mouse serum solution on the RGO surface. We also performed a comparative experiment of applying crude cell lysate or mouse serum solution lacking anti-BSA antibody on the dBSA-treated RGO surfaces, which results in a negligible ΔR_{ct}, indicative of no specific and/or nonspecific binding between the electrode and the other biomolecules. Notably, this characteristic imparts a great advantage of excluding the mandatorily applied backfill process used in the conventional biosensors to avoid the nonspecific binding of contaminants on the surface.

CONCLUSIONS

In summary, this study presents a novel means of utilizing π-stacking interactions in graphene-based impedance sensors for the best use of structural characteristic of graphenes comprising interconnected aromatic carbons. As a graphene surface, instead of using CVD-grown graphene layer with low electrical resistance, RGO films prepared by layer-by-layer assembly of charged GO nanosheets are used, on which the interfacial hopping transport of electrons beneficially works for enhancing the signal response in EIS data and results in a greater sensitivity by an order of magnitude compared to the case of CVD-grown graphenes. For inducing the π-stacking interactions on the RGO surface, biomolecules should have relevant hydrophobicity on their surface, for which the denaturation approach of protein probes of BSA has been pursued as a demonstrative example. For denaturation, the thermal method is utilized for obtaining highly dense and uniform coverage of BSA on RGO surface. As a result, tens of femtomolar (25 fM) sensitivity for anti-BSA antibody has been confirmed with EIS measurements with the suggested sensing platform. A notable performance can be attributed to the characteristic of the π-stacking interactions between RGO substrate and probes that

do not require any chemical functionalities for inducing covalent binding. Furthermore, the added advantage of exclusion of a backfill process enables this approach to be used for versatile applications in biosensing devices. Since the π-stacking interactions can be harnessed for other types of protein probes or DNAs, the presented approach can be used as a versatile platform for the graphene-based biosensors.

■ ASSOCIATED CONTENT

Supporting Information

AFM observations of CVD-grown graphene surface before and after the dBSA binding. This material is available free of charge via the Internet at http://pubs.acs.org.

■ AUTHOR INFORMATION

Corresponding Author

*E-mail addresses: checws@skku.edu (W.-S.C.); pjyoo@skku.edu (P.J.Y.).

Notes

The authors declare no competing financial interest.

■ ACKNOWLEDGMENTS

This work was supported by research grants of NRF (2012M1A2A2671795), Global Frontier R&D Program on Center for Multiscale Energy System (2012M3A6A7055540), and Basic Science Research Program (2012-0009158) funded by the National Research Foundation under the Ministry of Science, ICT & Future, Korea.

■ REFERENCES

(1) Castro Neto, A. H.; Guinea, F.; Peres, N. M. R.; Novoselov, K. S.; Geim, A. K. *Rev. Mod. Phys.* **2009**, *81*, 109−162.
(2) Geim, A. K.; Novoselov, K. S. *Nat. Mater.* **2007**, *6*, 183−191.
(3) Mohanty, N.; Berry, V. *Nano Lett.* **2008**, *8*, 4469−4476.
(4) Wu, J. B.; Becerril, H. A.; Bao, Z. N.; Liu, Z. F.; Chen, Y. S.; Peumans, P. *Appl. Phys. Lett.* **2008**, *92*, 263302.
(5) Stoller, M. D.; Park, S. J.; Zhu, Y. W.; An, J. H.; Ruoff, R. S. *Nano Lett.* **2008**, *8*, 3498−3502.
(6) Kuila, T.; Bose, S.; Khanra, P.; Mishra, A. K.; Kim, N. H.; Lee, J. H. *Biosens. Bioelectron.* **2011**, *26*, 4637−4648.
(7) Robinson, J. T.; Perkins, F. K.; Snow, E. S.; Wei, Z. Q.; Sheehan, P. E. *Nano Lett.* **2008**, *8*, 3137−3140.
(8) Wang, K.; Ruan, J.; Song, H.; Zhang, J. L.; Wo, Y.; Guo, S. W.; Cui, D. X. *Nanoscale Res. Lett.* **2010**, *6*, 8.
(9) Varghese, N.; Mogera, U.; Govindaraj, A.; Das, A.; Maiti, P. K.; Sood, A. K.; Rao, C. N. R. *ChemPhysChem* **2009**, *10*, 206−210.
(10) Wang, Y.; Li, Z. H.; Hu, D. H.; Lin, C. T.; Li, J. H.; Lin, Y. H. *J. Am. Chem. Soc.* **2010**, *132*, 9274−9276.
(11) Cui, Y.; Kim, S. N.; Jones, S. E.; Wissler, L. L.; Naik, R. R.; McAlpine, M. C. *Nano Lett.* **2010**, *10*, 4559−4565.
(12) Kang, X. H.; Wang, J.; Wu, H.; Aksay, I. A.; Liu, J.; Lin, Y. H. *Biosens. Bioelectron.* **2009**, *25*, 901−905.
(13) Wan, Y.; Lin, Z. F.; Zhang, D.; Wang, Y.; Hou, B. R. *Biosens. Bioelectron.* **2011**, *26*, 1959−1964.
(14) Liu, J. B.; Fu, S. H.; Yuan, B.; Li, Y. L.; Deng, Z. X. *J. Am. Chem. Soc.* **2010**, *132*, 7279−7281.
(15) Du, D.; Zou, Z. X.; Shin, Y. S.; Wang, J.; Wu, H.; Engelhard, M. H.; Liu, J.; Aksay, I. A.; Lin, Y. H. *Anal. Chem.* **2010**, *82*, 2989−2995.
(16) Pumera, M. *Mater. Today* **2011**, *14*, 308−315.
(17) Zhou, M.; Zhai, Y. M.; Dong, S. J. *Anal. Chem.* **2009**, *81*, 5603−5613.
(18) Hu, Y. W.; Yang, T.; Wang, X. X.; Jiao, K. *Chem.—Eur. J.* **2010**, *16*, 1992−1999.
(19) Katz, E.; Willner, I. *Electroanalysis* **2003**, *15*, 913−947.
(20) Willner, I.; Zayats, M. *Angew. Chem.-Int. Edit.* **2007**, *46*, 6408−6418.
(21) Macdonald, J. R. *Impedance spectroscopy*; Wiley: New York, 1987.
(22) Chang, H. X.; Tang, L. H.; Wang, Y.; Jiang, J. H.; Li, J. H. *Anal. Chem.* **2010**, *82*, 2341−2346.
(23) Dubuisson, E.; Yang, Z. Y.; Loh, K. P. *Anal. Chem.* **2011**, *83*, 2452−2460.
(24) Jung, J. H.; Cheon, D. S.; Liu, F.; Lee, K. B.; Seo, T. S. *Angew. Chem.-Int. Edit.* **2010**, *49*, 5708−5711.
(25) Park, J. S.; Cho, S. M.; Kim, W. J.; Park, J.; Yoo, P. J. *ACS Appl. Mater. Interfaces* **2011**, *3*, 360−368.
(26) Li, D.; Muller, M. B.; Gilje, S.; Kaner, R. B.; Wallace, G. G. *Nat. Nanotechnol.* **2008**, *3*, 101−105.
(27) Yadav, P. K.; McKavanagh, F.; Maguire, P. D.; Lemoine, P. *Appl. Surf. Sci.* **2011**, *258*, 361−369.
(28) Ni, Z. H.; Wang, Y. Y.; Yu, T.; Shen, Z. X. *Nano Res.* **2008**, *1*, 273−291.
(29) Wu, Y. H.; Yu, T.; Shen, Z. X. J. *Appl. Phys.* **2010**, *108*, 071301.
(30) Li, H. Q.; Han, L. N.; Cooper-White, J. J.; Kim, I. *Nanoscale* **2012**, *4*, 1355−1361.
(31) Rao, F. B.; Almumen, H.; Fan, Z.; Li, W.; Dong, L. X. *Nanotechnology* **2012**, *23*, 105501.
(32) Kolusheva, S.; Kafri, R.; Katz, M.; Jelinek, R. *J. Am. Chem. Soc.* **2001**, *123*, 417−422.